

# Evaluation of electrochemical impedance spectra by the distribution of relaxation times

Ellen IVERS-TIFFÉE and André WEBER<sup>†</sup>

Institute for Applied Materials (IAM-WET), Karlsruhe Institute of Technology (KIT), Adenauerring 20b, D-76131 Karlsruhe, Germany

**Electrochemical impedance spectroscopy** is a well suited method for studying the properties of electrochemical systems. In recent decades electrochemical systems were investigated at different scales, from small model electrodes to high power devices, such as fuel cells and batteries. In the latter case, the measurement of reliable spectra and their evaluation is challenging because (i) the impedance is usually very low ( $\ll 1 \Omega$ ), (ii) there is more than one rate limiting, electrochemical process per electrode, (iii) their charge transfer and transport processes are coupled and (iv) cathodic and anodic contributions overlap in the frequency domain. The Distribution of Relaxation Times (DRT) is supportive when deconvoluting complex impedance spectra, and has therefore gained increased attention. In this paper we introduce selected results of advanced impedance analysis. We discuss the impact of impedance data quality, statistically distributed noise and single errors in the spectra. Furthermore, the applicability of DRT for establishing adequate equivalent circuit models for ceramic electrochemical devices, such as batteries and fuel cells will be discussed.

©2017 The Ceramic Society of Japan. All rights reserved.

Key-words : Impedance spectroscopy, Distribution of relaxation times, Solid oxide fuel cell, Lithium ion battery

[Received November 13, 2016; Accepted December 12, 2016]

## 1. Introduction

### 1.1 Electrochemical impedance spectroscopy

Impedance spectroscopy and frequency response analysis are powerful tools for investigating the electrical properties of electroceramic materials and devices. The first investigations into the frequency dependency of material properties as the dielectric polarization date back to the 19th century. The concept of determining the resistance of an electrolyte by AC-measurements, to eliminate the impact of electrode polarization, was first discussed in 1869.<sup>1)</sup> The related challenges in the evaluation of resistances by AC-measurements have been summarized in.<sup>2)</sup> Since that time we have also seen the development of the theoretical background of equivalent circuits,<sup>3)</sup> as well as the analysis of polarizable and non-polarizable electrodes by AC-methods, including models to describe their electrical behavior.<sup>4)</sup>

AC-measurements became more and more popular for the analysis of materials and electrodes in the following decades. Milestones include: the work of Cole and Cole, who analyzed dispersion and absorption in dielectrics by alternating current measurements<sup>5)</sup> and suggested the Cole-Cole plot as a graphical tool for analyzing impedance data, the analysis of the impedance of galvanic cells by Sluyters<sup>6)</sup> as well as the investigations of the polarization in solid zirconia electrolytes by Bauerle,<sup>7)</sup> who proved in his work that AC-measurements are useful for ceramic materials applied in batteries and fuel cells.

While the impedance in all previously cited papers was measured with homemade setups, the introduction of frequency response analyzers in the 1970's and software for impedance data analysis<sup>8),9)</sup> dramatically increased the application of impedance spectroscopy (Fig. 1).

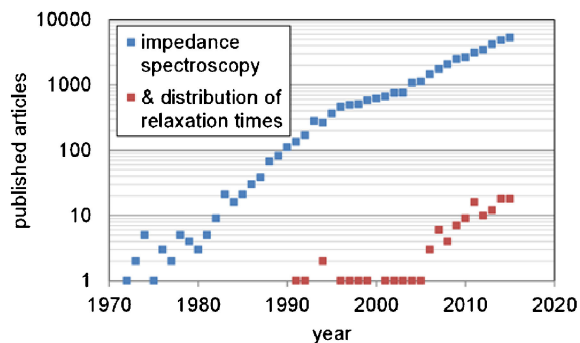


Fig. 1. Published articles on “impedance spectroscopy” and “impedance spectroscopy” & “DRT” listed in Scopus.

A review on the history of impedance spectroscopy is given in.<sup>10)</sup> The theory and many practical hints are discussed in the books of Macdonald,<sup>11),12)</sup> Orazem<sup>13)</sup> and Lasia.<sup>14)</sup> For a proper analysis of impedance spectra, including the distribution of relaxation times as discussed in the next chapters, any kind of error in the spectra should be carefully avoided. It is therefore recommended to follow the advice given in the chapters on impedance measurements, wiring of samples and errors in the above mentioned books, as well as in the manuals of the applied equipment. Furthermore, the testing of the validity of measured spectra is indispensable. Algorithms based on the Kramers-Kronig relation enable a detection of errors in the spectra.<sup>15),16)</sup> Appropriate software tools are available.<sup>17)</sup>

### 1.2 The distribution of relaxation times DRT

Despite the fact that the concept of a Distribution of Relaxation Times (DRT) was already introduced in 1907 for dielectrics and capacitors by Schiedler,<sup>18)</sup> and further developed by Wagner in

<sup>†</sup> Corresponding author: A. Weber; E-mail: andre.weber@kit.edu

<sup>‡</sup> Preface for this article: DOI <http://doi.org/10.2109/jcersj2.125.P4-1>

1913,<sup>19)</sup> the application of the DRT for the analysis of electrochemical impedance spectra was slow. There have been a number of publications where the DRT<sup>5),20)</sup> and approaches to unfold a DRT from impedance spectra are discussed.<sup>21)–27)</sup> In 2002 Schichlein<sup>28)</sup> published a methodology to calculate the distribution of relaxation times from solid oxide fuel cell impedance spectra. In his approach the deconvolution of the spectra enabled a high resolution of time constants.

The relation between the impedance spectrum  $Z(\omega)$  and the distribution of relaxation times  $\gamma(\tau)$ , which is for sake of simplicity often displayed as a distribution  $g(f)$  vs. the relaxation frequencies, is given by Eq (1).

$$Z(\omega) = R_0 + Z_{\text{pol}}(\omega) = R_0 + \int_0^\infty \frac{\gamma(\tau)}{1+j\omega\tau} d\tau \quad (1)$$

This relation is valid for any kind of system that fulfills the fundamental demands of impedance spectroscopy—linearity (at least within the stimulation amplitude), causality and time invariance, and is not limited to capacitive ones as derived in.<sup>29)</sup> Schichlein<sup>28)</sup> applied a discrete Fourier transformation to compute the DRT from the imaginary part of  $Z(\omega)$ . An appropriate extrapolation and filtering of the data is required to suppress numerical error amplification. Thus, the method becomes unsuitable for impedance spectra exhibiting greater errors or inductive artefacts at higher frequencies. Furthermore the selection of extrapolation and filtering parameters is crucial.

Sonn<sup>30)</sup> pointed out that the mathematical problem with the above mentioned approach arises from the inversion of Eq. (1), an ill posed problem (Fredholm integral<sup>31)</sup>) that requires special methods to be solved, in order to avoid false peaks and oscillations.<sup>32)</sup> The calculation of the DRT by a Tikhonov regularization, using the software package Ftikreg, significantly improved the quality and reliability of the DRT. The Ftikreg source code is available; for example, at.<sup>33)</sup> Details on the code and its application are given in a related paper by Weese.<sup>34)</sup> Whereas the discrete Fourier transform method included extrapolation and filtering with a number of parameters and settings that have to be properly chosen, the Tikhonov regularization only requires one important parameter, the regularization parameter  $\lambda$ , which determines the smoothness of the DRT. In the case of excellent data quality or synthetic data; a small regularization parameter can be used - for noisy data the regularization parameter has to be increased to suppress false peaks and oscillations in the DRT. Further details about the regularization are discussed in the next chapter.

Recently, a number of tools have been discussed for calculating the DRT from an impedance spectrum and applying the methodology for the analysis of fuel cells and batteries.<sup>35)–43)</sup>

As already shown by Cole and Cole,<sup>5)</sup> appropriate graphical representations of measured impedance data are essential to derive meaningful models and extract the related parameters. Different ways to display and analyze impedance spectra have been suggested. Usually the complex impedance spectrum  $Z(\omega)$  is displayed in Nyquist- or Bode-plots. Unfortunately, their resolvability of processes with quite similar relaxation frequencies is limited. In contrast to that, the DRT provides a higher resolution. The fundamental advantage of the DRT is visualized in **Fig. 2**, displaying an impedance spectrum for two processes (two RC-elements, each consisting of a resistance  $R$  in parallel to a capacitor  $C$ ) with the time constants  $\tau_1 = 2\tau_2$  [time constant  $\tau = R \cdot C = 1/(2\pi f_i)$ ]. It is obvious that neither the Nyquist- (a) nor the real- and imaginary-part vs. frequency plot (b) are able to visualize the existence of the two processes. In the analytically calculated<sup>20)</sup>

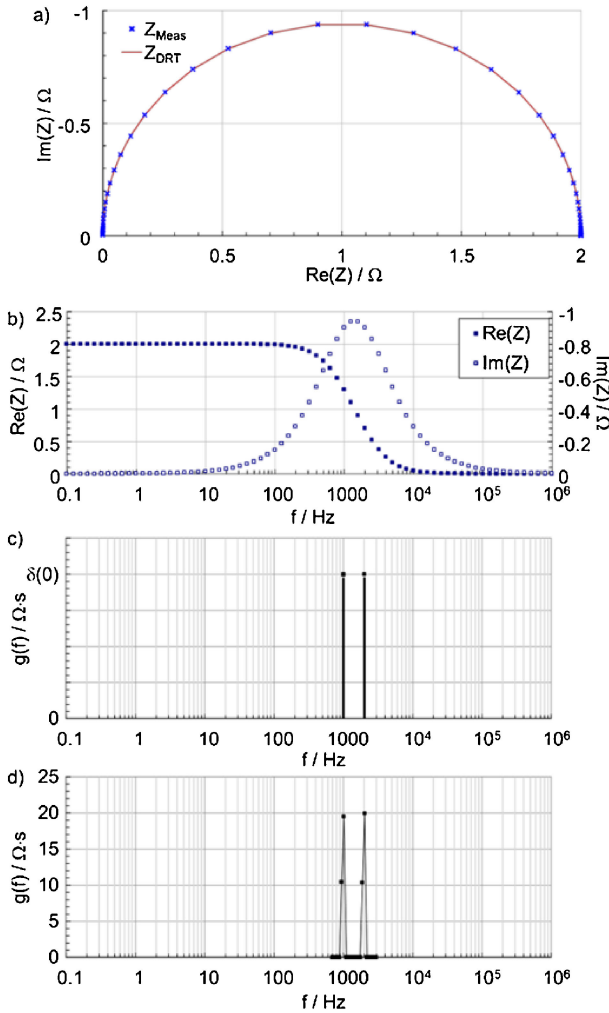


Fig. 2. An impedance spectrum of two RC-elements with the time constants  $\tau_1 = 2\tau_2$  displayed as Nyquist plot (a), real and imaginary part vs. frequency (b), analytical (c) and numerical DRT (d).

DRT (c) the two processes are represented by two Dirac-pulses, exactly located at the relaxation frequency of the processes. Such analytical calculation is not feasible in the case of discrete impedance values (i.e. any measured impedance spectrum where the type, resistance value and relaxation frequency of the processes are unknown). Thus, numerical methods as suggested in<sup>28)</sup> and<sup>30)</sup> are required. In the following, the latter approach will be used. The software package Ftikreg<sup>34)</sup> was applied to calculate the DRT from the real part of the related impedance spectrum  $Z(\omega)$ . The real part was chosen because it is less affected by measurement noise and errors. The result for the abovementioned example is shown in Fig. 2(d). In the case of the numerically calculated DRT of this spectrum, which is affected by the limited frequency range (100 mHz to 1 MHz) and resolution (10 points per decade), the two processes can be resolved.

This example demonstrates the advantage of the DRT. In an ideal (analytical) case the DRT transforms the broad peaks of the imaginary part of each RC-element into Dirac-pulses  $\delta(f_r-f)$  at the relaxation frequencies  $f_r$ ; in the case of discrete data, the peaks are drastically sharpened, enabling a deconvolution of processes with narrow relaxation times. The same holds for other equivalent circuit elements, such as an RQ-element (parallel connection of an ohmic resistance  $R$  and a constant phase element  $Q$ ) or a Warburg impedance. Even if such distributed elements

cannot be displayed as one discrete Dirac pulse, an improved resolution over the frequency axis is achieved.

The possibilities and limitations of applying the DRT will be discussed in the following sections. We will focus on the Tikhonov-regularization because this method enables a reliable calculation of the DRT with limited error sources and good stability vs. noise in the measured spectra. The impact of the regularization parameter and the impedance data quality will be discussed. Selected examples will show how the DRT can be applied to develop electrochemical models and analyze aging phenomena in fuel cells and batteries.

## 2. Tikhonov-regularization

The Tikhonov-regularization provides a solution for a minimization problem with smoothness as a secondary condition. It provides the fit to a model function that is smoothed by a regularization operator. The regularization parameter  $\lambda$  weights the regularization. The model function, in terms of an equivalent circuit model (ECM), corresponds to a serial connection of an infinite number of RC-elements. In the case of a numerical DRT, it is reduced to a finite number of RC-elements per decade, which determines the resolution and precision of the DRT and related models.<sup>44)</sup> The impact of  $\lambda$  on the DRT of an RC-element is displayed in Fig. 3. With decreasing regularization parameter  $\lambda$ , the peak in the DRT becomes higher and narrower. The resolution of the DRT is increased.

This is also visible in Fig. 4. The  $\lambda$ -value determines the resolution in the DRT. In the given example the two processes (two RC-elements with  $\tau_1 = 2\tau_2$ ) can be resolved for  $\lambda$ -values  $\leq 10^{-8}$ . It should be noted that the height and width of the peaks differ, which in principle should be similar; this is related to numerical issues in the DRT calculation.

Synthetic impedance spectra were used to calculate the DRT in the previous figures. The spectra were free of measurement errors and noise. Since they consist of discrete values with a limited frequency range and resolution, the DRT calculation is only

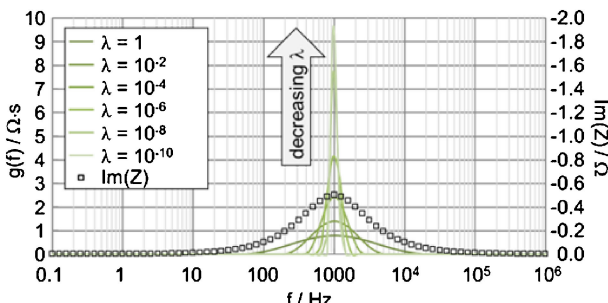


Fig. 3. DRTs of an RC-element calculated by the Tikhonov-regularization using different  $\lambda$ -values.

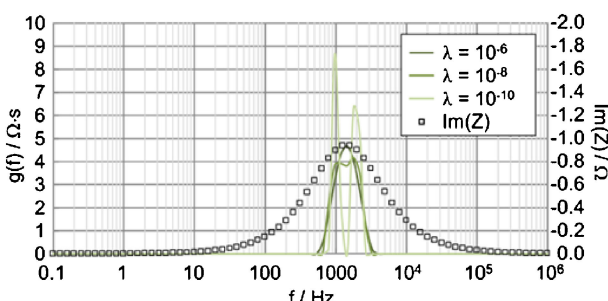


Fig. 4. DRTs of a spectrum consisting of two RC-elements with  $\tau_1 = 2\tau_2$  (similar to Fig. 2), calculated with 3 different  $\lambda$ -values.

affected by the “incompleteness” of the spectra and numerical errors. On the other hand, measured spectra are usually affected by electrical noise alongside other errors related to the test bench and the cell. Therefore, the impact of such measurement errors on the DRT has to be considered. An example is shown in Fig. 5. The synthetic spectrum (consisting of a series resistance and an RC-element) was disturbed by adding statistically distributed noise.

Despite the obvious errors in the spectra, which would usually prohibit any further analysis of the data, the DRTs do not differ significantly (whether with or without noise). This has to be related to the statistical distribution of the error, which is compensated by the regularization. Additional peaks only appear at the borders of the spectrum and are caused by the large number of data points. These do not contain any information about polarization processes but are only noise.

Figure 6 displays the DRTs of a spectrum consisting of a series resistance and two RC-elements with narrow relaxation frequencies similar to Fig. 4. If the noise is added to the spectrum, the two resolvable peaks merge into one. Further on, an additional artificial peak is observed at higher frequencies. Such behavior is typical for the DRTs of erroneous spectra. Noise in the spectra reduces the resolution and can even create artificial peaks in the DRT.

In comparison to statistically distributed errors, which are smoothed by the regularization and thus eliminated in the DRT, single erroneous data points in the spectrum can have a severe impact on the DRT. This type of error is typical for the mains frequency of 50 Hz. The synthetic spectrum in Fig. 7 contains a single erroneous data point, which results in an additional small peak, as well as a shift in the frequency and size of the main peaks in the DRT. Since such erroneous data points can easily be detected, it is possible to remove them before the DRT is calculated. The missing data point does not have a remarkable impact on the DRT.

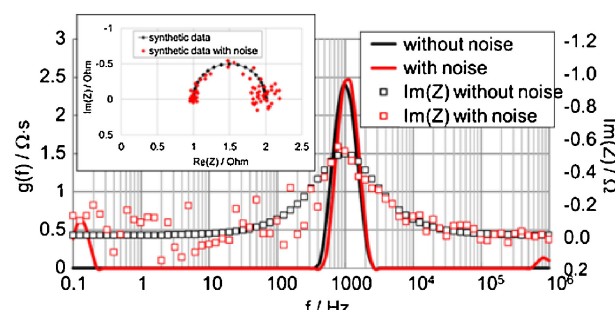


Fig. 5. DRTs of the spectra of a single RC-element with and without noise ( $\lambda = 10^{-8}$ ).

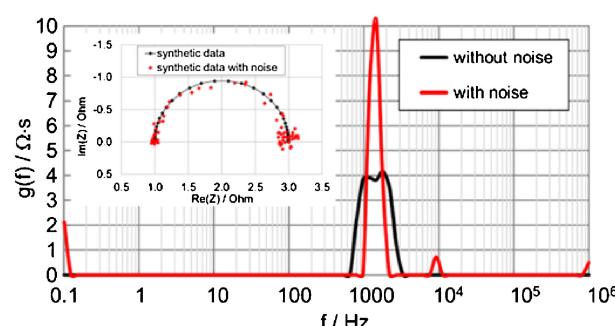


Fig. 6. DRTs of the spectra of two RC-elements ( $\tau_1 = 2\tau_2$ ) with and without noise ( $\lambda = 10^{-8}$ ).

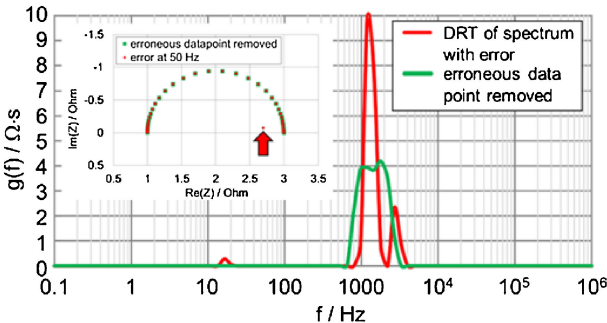


Fig. 7. DRTs of a spectrum of two RC-elements ( $\tau_1 = 2\tau_2$ ) with one erroneous data point at 50 Hz ( $\lambda = 10^{-8}$ ). Removing this data point from the spectrum removes the errors in the DRT.

The previous examples show that the DRT powerfully deconvolutes impedance spectra. As long as the DRT analyzes high quality impedance data, the error level is low. Any kind of noise or errors in the spectra can have a severe impact on the calculated DRT. Possible errors are a reduced resolution or artificial peaks, as well as a shift in frequency and size of peaks. The quality of the measured impedance spectra is therefore essential for the applicability of the DRT.

Also, the choice of a proper  $\lambda$ -value is strongly tied to the quality of an impedance spectrum. Generally speaking, the  $\lambda$  should be chosen to be as small as possible for good resolvability and as large as needed to suppress artifacts. The decision of what is an artifact and what is information can only be facilitated by repeated measurements with varying conditions and by observing which parts of the DRT show physically meaningful behavior and which just randomly vary. Since many errors can influence a measurement, and thus a DRT, we consider such procedures to be the only way of determining a meaningful value of lambda. All automatic procedures will produce false confidence in the achieved DRT - which is not generally justified. Hanke, who examined the problem of regularization techniques from a mathematician's point of view, stated that, "No black-box procedures for choosing the regularization parameter  $\lambda$  are available, and most likely will never exist".<sup>45)</sup>

A further point that has to be considered in the application of the DRT is the type of processes to be analyzed. RC-elements are rare in measured spectra. In electrochemical systems RQ-, Gerischer and Warburg elements are more likely. The following will show the analytical form of the DRT of these equivalent circuit elements. More details on the analytical calculation of the DRT of these equivalent circuit elements and a comparison of the analytical and numerical result are discussed in.<sup>46)</sup>

The impedance of an RQ-element (the parallel connection of resistance and constant phase element Q) is given by:

$$Z_{RQ}(\omega) = \frac{R}{1 + RQ^{-1}} \quad (2)$$

with the constant phase element Q:

$$Z_Q(\omega) = Q(\omega) = \frac{1}{(j\omega)^{n_Q} Y_Q} \text{ with } 0 \leq n_Q \leq 1 \quad (3)$$

As derived in<sup>28)</sup> the analytical DRT of the RQ-element is given by Eq. (4) [with  $x = \ln(\omega)$ ]:

$$g_{RQ}(x) = \frac{R_{pol}}{2\pi} \frac{\sin[(1-n_Q)\pi]}{\cosh(n_Q x) - \cos[(1-n_Q)\pi]} \quad (4)$$

**Figure 8** shows this DRT for different  $n_Q$ -values. For  $n_Q = 1$  the RQ-element becomes an RC-element and thus a Dirac pulse

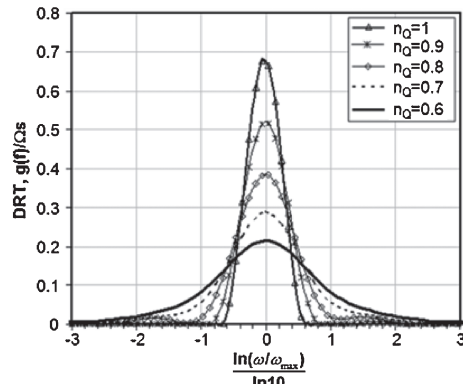


Fig. 8. Analytical DRT of an RQ-element according to Eq. (4) with different  $n_Q$ -values.<sup>46)</sup>

in the DRT. With decreasing  $n_Q$  the height of the peak decreases and its width increases.

The finite length Warburg element:

$$Z_{G-WL}(\omega) = R_W \cdot \frac{\tanh[(j\omega T_W)^{n_W}]}{(j\omega T_W)^{n_W}} \quad (5)$$

is highly asymmetric, and exhibits a rather complex analytical equation for its DRT:<sup>46)</sup>

$$g_{G-WL}(x)$$

$$= -\frac{R_W}{\pi} \left\{ \begin{array}{l} \frac{1}{2} e^{-\frac{j\pi+2x}{2n_W}} \cdot \frac{1}{\sqrt[n_W]{T_W}} \operatorname{sech}(\sqrt[n_W]{e^{j\pi} T_W}) \\ \cdot \operatorname{sech}(\sqrt[n_W]{e^{j\pi+x} T_W}) \\ = \left[ \begin{array}{l} \cos\left(\frac{\pi}{2n_W}\right) \cdot \sin\left(2\sqrt[n_W]{j e^{j\pi} T_W} \sin\left(\frac{\pi}{2n_W}\right)\right) \\ - \sin\left(\frac{\pi}{2n_W}\right) \sinh\left(2\sqrt[n_W]{j e^{j\pi} T_W} \cos\left(\frac{\pi}{2n_W}\right)\right) \end{array} \right] \\ - \frac{1}{2} j \frac{1}{\sqrt[n_W]{e^{j\pi} T_W}} \left( \tanh(\sqrt[n_W]{e^{j\pi} T_W}) \right. \\ \left. - e^{\frac{j\pi}{n_W}} \tanh(\sqrt[n_W]{e^{-j\pi+x} T_W}) \right) \end{array} \right\} \quad (6)$$

It has to be considered that there is not just one large peak located at the characteristic frequency but also a number of smaller, additional peaks at higher frequencies (Fig. 9). Thus, the generalized statement that each peak in the DRT corresponds to one physicochemical process in the investigated sample cannot be maintained. Asymmetric equivalent circuit elements, such as Warburg and Gerischer, exhibit several peaks in their DRT, which therefore extends over a wide frequency range of several decades. This impedes the deconvolution of spectra because an overlap with other physicochemical processes is more likely. Appropriate measures are required to resolve a minor process located in the similar frequency range (e.g. the second peak in the DRT of a Gerischer element). A preferable solution for this problem is to shift the relaxation frequencies of the processes by selecting appropriate operating parameters, as shown in.<sup>47)</sup>

A similar behavior is observed for the Gerischer element:

$$Z_G(\omega) = \frac{R_{chem}}{\sqrt{1 + j\omega t_{chem}}} \quad (7)$$

with the corresponding DRT, a complex valued function with a singularity at  $x = \ln(1/t_{chem})$ :

$$\tilde{g}_G(x) = \frac{\sqrt{2}R_{chem}}{\pi} \sqrt{\frac{(\sqrt{1 - (e^{xt_{chem}})^2} - 1)}{1 - (e^{xt_{chem}})^2}} \quad (8)$$

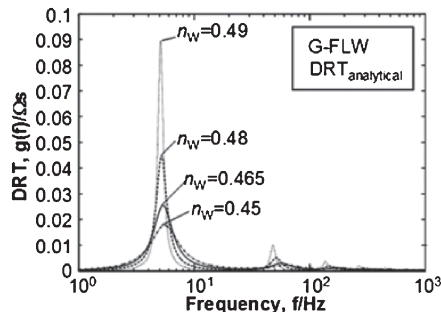


Fig. 9. Analytical DRT of a finite length Warburg element according to Eq. (6) with different  $n_W$ -values.<sup>46)</sup>

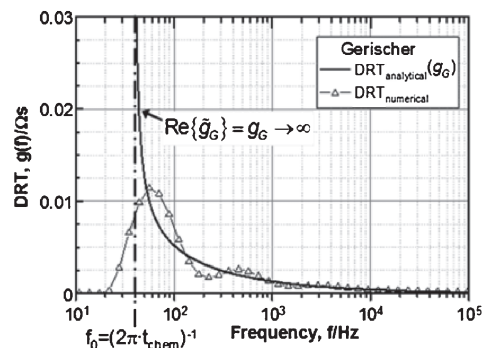


Fig. 10. Analytical [according to Eq. (9)] and numerical DRT of a Gerischer-element.<sup>46)</sup>

which can be simplified<sup>46)</sup> to:

$$g_G(x) \approx \begin{cases} \operatorname{Re} \left\{ \frac{\sqrt{2} R_{\text{chem}}}{\pi} \sqrt{\frac{(\sqrt{1 - (e^x t_{\text{chem}})^2} - 1)}{1 - (e^x t_{\text{chem}})^2}} \right\} & \text{for } x \geq \ln\left(\frac{1}{t_{\text{chem}}}\right) \\ 0 & \text{for } x < \ln\left(\frac{1}{t_{\text{chem}}}\right) \end{cases} \quad (9)$$

In Fig. 10 analytical and numerical DRT of a Gerischer element are displayed. Leonide pointed out that a more detailed mathematical treatment of Eq. (9) would probably deliver a more definitive conclusion about the correct analytical DRT-expression of a Gerischer-impedance.<sup>46)</sup>

### 3. Application of the DRT

This chapter will discuss a number of examples for the application of the DRT in the field of batteries and fuel cells. There are two different approaches for applying the DRT. The first is, a black box model approach based on the DRT, which is applicable for an experimental modeling of dynamic systems. This approach is useful for diagnosis purposes because it can be implemented in control algorithms or dynamic system models that do not require any information about the physicochemical background of the cell. In the second, the DRT can be applied to identify the different processes in a complex electrochemical system, thereby providing the basis for a detailed physicochemical model. Furthermore, there are applications using a combined CNLS-fit including the DRT as an additional quality criterion as well as the application of the DRT in durability investigations.

#### 3.1 The DRT in black box models

As shown in<sup>29)</sup> and<sup>48)</sup> the DRT includes a comprehensive representation of the dynamics of the analyzed system. Thus a

DRT-based model is applicable to predict the dynamic behavior of the system, as long as nonlinear effects are negligible. This approach – in a simplified form – is already state of the art in battery modeling. Models consisting of a small number of RC-elements, whose parameters are experimentally determined, are used in battery management systems. In<sup>44)</sup> a DRT based model was developed to simulate the electrical behavior of a battery during dynamic cycling. In this model the peaks of the DRT do not have to be assigned to physicochemical processes in the cell; the elements of the discrete DRT are directly used in the model. This enables a fully automated parameterization of the model, the measurement results can be directly converted into the required model parameters. Furthermore; no elements of fractional nature (constant phase, Warburg, Gerischer), which cannot be simulated directly in the time domain, are required. This, and the possibility of adjusting the model order, i.e. the number of RC-elements per decade, reduces the required computing power and enables real time simulations.

### 3.2 DRT-analysis of fuel cells and batteries

The impedance of high performance batteries and fuel cells usually contains a number of physicochemical processes related to different loss mechanism in the cathode, electrolyte, anode and their interfaces. In comparison to model electrodes, which are often dominated by a single rate determining step, the different resistance contributions can be quite similar in size and usually overlap in the frequency domain. In order to develop a physicochemical equivalent circuit model of the analyzed cell, the measured spectra have to be deconvoluted to identify all performance-related polarization processes.

Commonly, a small number of spectra are analyzed by a Complex Nonlinear Least Squares (CNLS) fit to an equivalent circuit model (ECM),<sup>9)</sup> which needs to be defined a priori. In many cases, existing ECMs are just copied and fitted to the spectra of the cell under investigation, without considering that even small differences in cell design and production parameters can have a severe impact on the electrochemistry of the cell. The problem of this approach is that any measured spectrum can be described by different ECMs. Complex ECMs, with their many free parameters, can be easily fitted to a measured spectrum. Very often this leads to a severe ambiguity of the adopted ECMs.<sup>11)</sup> It should be here noted that the discrete DRT also represents an ECM consisting of a large number (~100) of RC-elements in series. As most spectra can be described by their DRT,<sup>29)</sup> the DRT is a valid ECM but not a valid physicochemical model. The individual resistance values and time constants representing a DRT cannot be directly related to physicochemical processes in the cell.

To overcome that disadvantage the ECM (as well as the required starting values for a CNLS-fit) can be obtained by a pre-identification via the DRT. The DRT approach is particularly advantageous for the analysis of technical cells and stacks, where reference electrodes are not applicable for the separation of anode and cathode losses.

To deconvolute the different physicochemical processes in the impedance spectrum of an electrochemical cell, their different dependencies on operating parameters have to be considered. Such dependencies can be used to identify the nature of semi-circles in the spectrum or, with an even higher resolution, peaks in the DRT. In the case of fuel cells, one can easily vary the operating temperature, cathode and anode gas compositions, and current density. Moreover, the selected poisoning of electrodes or variations in electrode microstructure and thickness are possible measures to identify physicochemical processes in the spectra.

In<sup>30</sup> and<sup>49</sup> a combination of operating parameter variation and DRT-analysis of the measured spectra was applied to develop models for nickel/yttria stabilized zirconia (YSZ) cermet electrodes and anode supported solid oxide fuel cells (SOFCs). The DRT of impedance spectra measured during a stepwise variation of only one operating parameter, while keeping all the other operating parameters constant, enabled the identification of the only differing loss mechanism in the spectrum. Based on this pre-identification by the DRT, a physicochemically meaningful ECM was developed and parameterized by CNLS-fits. The suggested methodology usually requires the measurement of a rather large number of spectra. This is because each possible operating parameter set should be analyzed and the step-size should be kept small during each parameter variation. In the case of an SOFC operated with air as the oxidant and H<sub>2</sub>/H<sub>2</sub>O-mixtures as the fuel, it is possible to vary temperature, the oxygen partial pressure (pO<sub>2</sub>) at the cathode and the hydrogen and steam partial pressures (pH<sub>2</sub>, pH<sub>2</sub>O) at the anode. Assuming a number of 10 spectra per variation, which in most cases provides sufficient resolution, the number of possible operating parameter sets (and thus the number of spectra to be measured) would be 10<sup>4</sup>. It is obvious that this approach is not feasible and that the number of operating parameter sets has to be significantly reduced. The question is how to find the operating parameter sets which provide the best resolution for each physicochemical process in the cell.

One approach is to minimize the impact of all other processes. To do this, the natures of the different processes have to be considered. If, for example, the gas diffusion in the anode substrate of an SOFC is of interest, the gas diffusion in the cathode can be eliminated by using oxygen instead of air. All processes related to electrochemical reactions at the cathode and the anode are usually thermally activated, whereas gas diffusion is practically independent of temperature, or may even slightly increase with increasing temperature.<sup>50</sup> Thus, a high operating temperature should be selected to suppress the impact of these processes in the spectra. Furthermore an appropriate parameter variation has to be selected. To do this we must consider the impact of the different operating parameters on the impedance of the process under investigation. In the case of the gas diffusion in the anode substrate, which can be described by the finite length Warburg element according to Eq. (5), the resistance R<sub>W</sub> shows parameter dependencies according to Eq. (10):

$$R_W = \left( \frac{RT}{2F} \right)^2 \frac{L_{an}}{D_{H_2O,H_2}^{\text{eff}}} \left( \frac{1}{pH_2} + \frac{1}{pH_2O} \right)^{-1} \quad (10)$$

In this equation we can find some constants with their usual meaning (R, F), the temperature T, the diffusion length L<sub>an</sub> (thickness of the substrate), and the effective (temperature dependent) diffusion coefficient:

$$D_{H_2O,H_2}^{\text{eff}} = \frac{\varepsilon}{\tau} D_{H_2O,H_2} \quad (11)$$

which is affected by the porosity  $\varepsilon$  and tortuosity  $\tau$  of the substrate and the fuel gas composition (pH<sub>2</sub>, pH<sub>2</sub>O). Examined in more detail, the gas composition will have a significant impact on R<sub>W</sub>. Especially for pH<sub>2</sub>O → 0 or pH<sub>2</sub> → 0 (the latter is not suggested, due to stability reasons), the resistance will be dominated by this process. Thus, the hydrogen to steam ratio variation would be an appropriate choice for analyzing this process. This approach provides physicochemically meaningful parameters: the porosity to tortuosity relation, as shown in.<sup>49</sup> Such parameters are not only valid for impedance models; they can be directly applied in other electrochemical models, as shown in.<sup>51,52</sup>

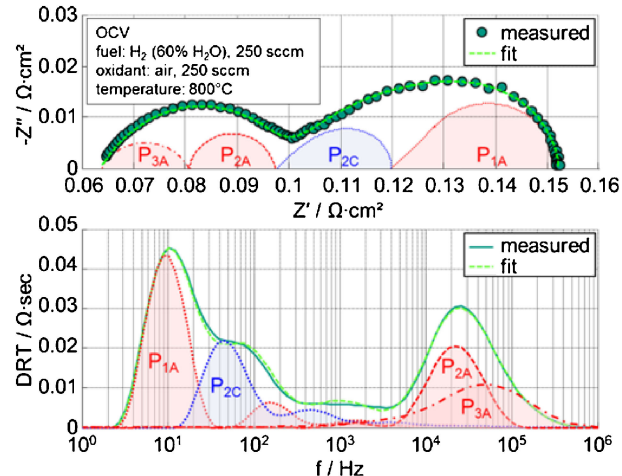


Fig. 11. Impedance spectrum and DRT of an anode supported SOFC. The different processes occurring at the cathode (blue) and at the anode (red) are plotted in the diagrams.

More details on how to pre-identify the different physicochemical processes in a cell from impedance spectra and how to set up meaningful ECMs can be found in<sup>46</sup> for SOFCs and in<sup>53</sup> for lithium ion batteries. The cell models and their components are quite versatile and can be extended and used for different types of electrodes or cells.<sup>54–57</sup>

In the case of the SOFC-model, Leonide performed a number of parameter variations to identify the different processes in the cell. By selecting appropriate testing conditions the number of spectra required to set up and validate the model could be reduced to several hundred, much lower than the 10<sup>4</sup> possible combinations. **Figure 11** shows the application of the model to the spectrum of an anode supported SOFC (ASC). The model is composed of the following processes:

P<sub>1A</sub>: gas diffusion in the anode substrate (including contact mesh and anode flowfield) described by a finite length Warburg element

P<sub>2A</sub>&P<sub>3A</sub>: coupling of H<sub>2</sub>-electro-oxidation, ionic transport and gas diffusion in the anode functional layer (AFL), approximated by two RQ-elements

P<sub>1C</sub>: gas diffusion in the cathode (including contact mesh and cathode flowfield), approximated by an RQ-element (only at pO<sub>2</sub> ≪)

P<sub>2C</sub>: oxygen reduction in a mixed ionic-electronic conducting cathode described by a Gerischer element

It is obvious that P<sub>1A</sub> and P<sub>2C</sub> are strongly overlapping. Nevertheless, a CNLS-fit is possible because both processes are represented by physicochemically meaningful ECMs. It should be noted that the high resolution of the DRT can also be utilized within a CNLS-fit. By including the DRT as an additional quality criterion, the stabilization of the fitting procedure and the consistency check of the result improves the reliability of the fitting results.<sup>48</sup>

In<sup>58</sup> Kromp extended the existing model to more complex, reformate fuels. His analysis used a similar approach and revealed that in typical reformate compositions only hydrogen is directly electrochemically oxidized, whereas carbon monoxide is converted by the water-gas shift reaction (WGS), creating an additional process at low frequencies. By adding small amounts (0.5 ppm) of H<sub>2</sub>S to the fuel it was possible to prove that the low frequency process is related to a CO-conversion by the WGS.<sup>59</sup> **Figure 12** displays an example of the DRT alteration during

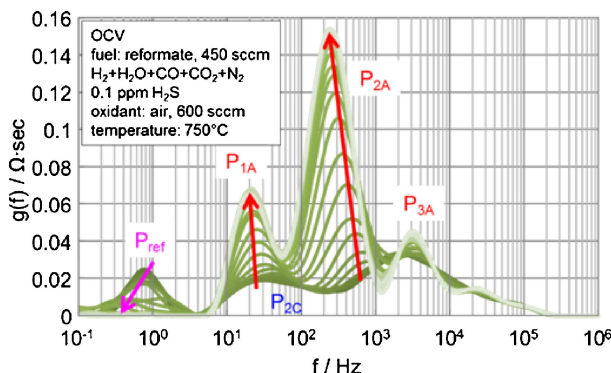


Fig. 12. DRTs during sulfur poisoning of an anode supported SOFC, operated with a reformatte fuel.

sulfur poisoning. The low frequency process  $P_{\text{ref}}$ , which is attributed to the coupling of CO/CO<sub>2</sub>-gas diffusion and the WGS on the nickel surfaces (which is deactivated by the sulfur-species in the fuel), decreases. However,  $P_{1A}$  ( $\text{H}_2/\text{H}_2\text{O}$ -gas diffusion) and  $P_{2A}$  as well as  $P_{3A}$  (hydrogen electrooxidation in the AFL) increase.

It should be pointed out that the selection of operating parameters for such types of impedance and DRT analysis should not be limited to technologically meaningful parameters. Although nobody would operate a SOFC system with pure oxygen or a highly diluted fuel, such tests at far-beyond-standard operating conditions can be extremely helpful when analyzing electrochemistry and deconvoluting the different loss mechanisms.

Recently, Leonide's model was modified by implementing a transmission line model (TLM) instead of two RQ-elements  $P_{2A}$  and  $P_{3A}$ .<sup>60)</sup> The TLM is capable of describing the coupling of H<sub>2</sub>-electrooxidation and ionic transport in the AFL in a physicochemical meaningful way. The parameterization of this model was supported by combining (i) microstructural parameters evaluated by means of FIB/SEM-tomography,<sup>61)</sup> (ii) the line specific resistance of the triple phase boundary (TPB) determined by electrochemical impedance spectroscopy (EIS) on patterned model anodes,<sup>62)</sup> (iii) the conductivity of the YSZ-matrix including the impact of NiO interdiffusion<sup>63),64)</sup> and (iv) the DRT as an additional quality criterion in the fitting procedure.<sup>48)</sup> Please note, without considering the above mentioned parameters, a fitting of the spectra with even lower error levels would be possible. Unfortunately, the results are no longer unambiguous. If such complex models are considered it is recommended to include as many parameters determined in separate experiments as possible, and to apply the DRT as an additional criterion in the fit or at least compare DRTs of measured spectra and the fitting result. This can be illustrated by the two TLMs exhibiting a similar overall polarization resistance but different values of ionic conductivity and TPB-resistance in Fig. 13. While only small differences are visible in the Nyquist plot, the DRT is able to clearly resolve the differences in the TLM.

Besides solid oxide fuel cells, the DRT-approach was successfully applied for the analysis of lithium ion batteries. Electrodes, which have been characterized in experimental cells<sup>65),66)</sup> and commercial cells,<sup>67)</sup> were investigated. A general problem in the impedance analysis of lithium ion batteries is that the conditions at cathode and anode cannot be independently varied. While independently controlling the activity of the reactants and reaction products at both electrodes is feasible for the related gas composition in a fuel cell, it is impossible in a lithium ion battery.

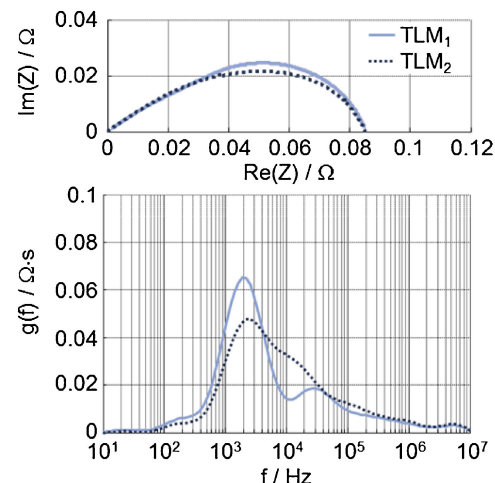


Fig. 13. Impedance spectra and DRTs of different parameterized TLMs with a similar overall polarization resistance but different values of ionic conductivity and TPB-resistance.

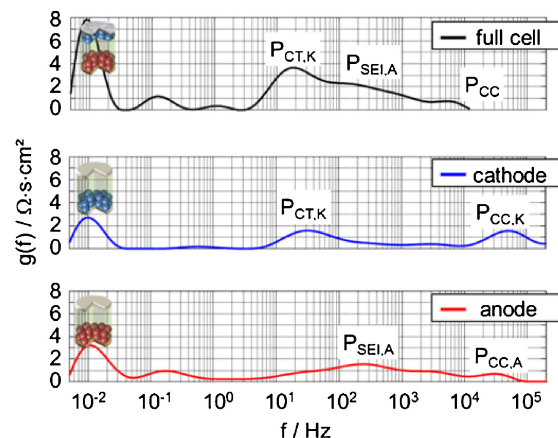


Fig. 14. DRT of the full cell (commercial Kokam pouch cell) in comparison to the DRTs of harvested anodes and cathodes investigated in experimental Li-ion batteries with reference electrode.

Therefore, symmetrical cells or "half" cells with a Li-metal counter electrode and a reference electrode, are required. In<sup>67)</sup> the model for a 18650 cell was developed by a comparison of the full cell impedance with experimental cells made of harvested 18650 cell materials. This approach allowed an identification of the physicochemical processes in the impedance spectrum of the 18650 cell. Temperature and state of charge dependencies were evaluated and the processes could be assigned to anode and cathode (Fig. 14).

It has to be considered that the low frequency part of the spectrum of a lithium ion battery is affected by the capacitive branch related to the coupling of diffusion in the active materials and the differential capacity. These processes are usually very slow and thus require time-consuming measurements at very low frequencies < 1 mHz. One approach to solving this problem is discussed in.<sup>68)</sup> The capacitive branch was first fitted to an ECM consisting of a Finite Length Warburg element and a serial capacitor<sup>69)</sup> and then subtracted from the spectra before DRT-calculation. Another approach is to measure the spectra down to the  $\mu\text{Hz}$ -range by time domain methods.<sup>70)</sup>

In<sup>71)</sup> Illig developed a TLM for the graphite anode of a lithium ion battery. The fitting of the complex impedance model was

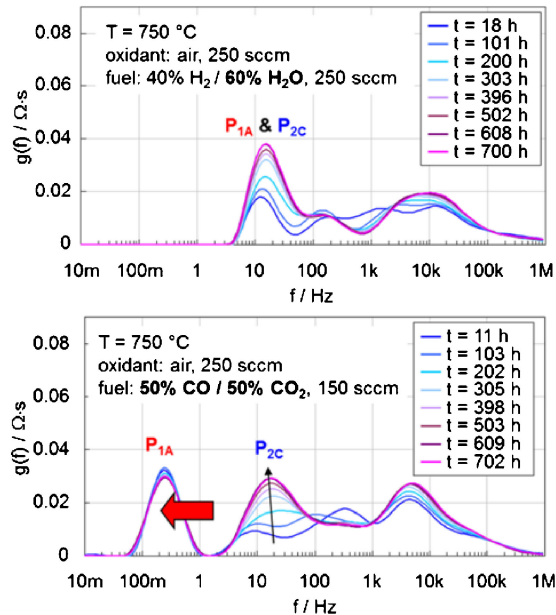


Fig. 15. DRTs of impedance spectra of an anode supported SOFC measured in  $\text{H}_2/\text{H}_2\text{O}$  and  $\text{CO}/\text{CO}_2$  fuel during a durability test of 1000 h.

supported by (i) the DRT, (ii) the separately measured electronic conductivity<sup>72)</sup> and (iii) microstructure parameters,<sup>73)</sup> which were evaluated by means of X-ray tomography analysis ( $\mu\text{CT}$ ). Thus, the number of free model parameters in the fit was reduced. Despite the complexity of the ECM, this approach enabled a stable CNLS-fit.

### 3.3 DRT-analysis of degradation phenomena

Due to its high resolution, the DRT is an excellent tool for displaying degradation phenomena in electrochemical cells. Endler<sup>47)</sup> investigated the degradation processes in anode supported cells. Durability tests over 1000 h of operation revealed that a major part of the degradation has to be attributed to the LSCF-cathode ( $\text{La}_{0.58}\text{Sr}_{0.4}\text{Co}_{0.2}\text{Fe}_{0.8}\text{O}_{3-\delta}$ ). In the investigated cells the cathode's polarization resistance is initially very small and covered by the gas diffusion process in the substrate. The gas diffusion process was shifted to lower relaxation frequencies by exchanging the usually applied  $\text{H}_2/\text{H}_2\text{O}$  fuel mixture for  $\text{CO}/\text{CO}_2$ . This revealed the cathode polarization process. Figure 15 compares the DRTs of spectra in  $\text{H}_2/\text{H}_2\text{O}$  and  $\text{CO}/\text{CO}_2$  measured during a durability test. It is obvious that the test in hydrogen/steam cannot provide information about the underlying degradation mechanisms. The overlapping of  $P_{1A}$  (gas diffusion in the anode substrate) and  $P_{2C}$  (oxygen reduction in the LSCF-cathode) rules out a reliable CNLS-fit of the spectra. A temporary change of the fuel composition to a  $\text{CO}/\text{CO}_2$  mixture reveals that the degradation has to be attributed to the cathode, whereas the gas diffusion resistance in the anode substrate slightly decreases with time. This approach even allows one to determine the temporal behavior of material parameters such as the surface exchange and oxygen diffusion coefficient of LSCF.<sup>74)</sup>

Since then, the analysis of degradation phenomena by means of the DRT was applied in a number of studies. In<sup>75),76)</sup> chromium poisoning effects were analyzed, while<sup>77)</sup> reveals details about sulfur poisoning of Ni/YSZ cermet anodes,<sup>78)</sup> provides information about the excellent redox stability of strontium titanate based ASCs and<sup>79)</sup> discusses the performance and stability of SOFCs operated in a biogas fuel. The DRT analysis revealed an impact

on the hydrogen electrooxidation in the AFL ( $P_{2A}, P_{3A}$ ) and an increase in the gas diffusion polarization ( $P_{1A}$ ), both attributed to carbon deposition in the AFL and the substrate. A similar behavior was observed in.<sup>40)</sup> In<sup>35)</sup> performance and durability during co-electrolysis of fuel electrode supported cells was investigated. The degradation of a short stack operated in fuel cell and electrolysis mode was evaluated by EIS and DRT at the Research Center Jülich.<sup>80)</sup> Sumi analyzed the degradation mechanisms in microtubular SOFCs.<sup>37)</sup> In all of these studies the DRT increased the resolution and enabled a more accurate description of aging mechanisms.

### 4. Summary

The evaluation of Electrochemical Impedance Spectra by the Distribution of Relaxation Times is beneficial for the analysis of ceramic electrochemical devices, such as batteries and fuel cells. The last decade saw an increase of DRT application to deconvolute the impedance spectra of complex electrochemical systems, such as batteries and fuel cells. It has been shown that the DRT not only visualizes the individual polarization processes in a spectrum but also provides significant advantages in equivalent circuit modeling and can even improve the stability and reliability of CNLS-fitting.

However, it should not be concealed that a reliable DRT calculation requires high quality impedance data, as well as sufficient experience in selecting appropriate parameters for filtering, extrapolation or regularization. The DRT is not an algorithm that can simply be applied to deconvolute any kind of impedance spectrum.

Setting up comprehensive electrochemical models of fuel cells and batteries requires a sufficient number of parameter variations, excellent impedance data quality and an appropriate use of DRT-algorithms. A valid model should be able to reproduce the measured impedance values for any combination of operating parameters.

### References

- 1) F. Kohlrausch and W. A. Nippoldt, *Ann. Phys.*, **214**, 280–298 (1869).
- 2) F. Kohlrausch, *Ann. Phys.*, **285**, 225–256 (1893).
- 3) O. Heaviside, "Electromagnetic Theory", Macmillan & Co., London (1894).
- 4) E. Warburg, *Ann. Phys.*, **303**, 493–499 (1899).
- 5) K. S. Cole and R. H. Cole, *The Journal of Chemical Physics*, **9**, 341–351 (1941).
- 6) J. H. Sluyters, *Recueil des Travaux Chimiques des Pays-Bas—Journal of the Royal Netherlands Chemical Society*, **79**, 1092–1100 (1960).
- 7) J. E. Bauerle, *J. Phys. Chem. Solids*, **30**, 2657–2670 (1969).
- 8) J. R. Macdonald and J. A. Garber, *J. Electrochem. Soc.*, **124**, 1022–1030 (1977).
- 9) B. A. Boukamp, *Solid State Ionics*, **20**, 31–44 (1986).
- 10) D. D. Macdonald, *Electrochim Acta*, **51**, 1376–1388 (2006).
- 11) J. R. Macdonald, "Impedance Spectroscopy", John Wiley & Sons, New York (1987).
- 12) E. Barsoukov and J. R. Macdonald, "Impedance Spectroscopy: Theory, Experiment, and Applications", 2ed., Wiley-Interscience, Hoboken NJ (2005).
- 13) M. E. Orazem and B. Tribollet, "Electrochemical Impedance Spectroscopy", John Wiley & Sons, Inc., Hoboken, NJ (2008).
- 14) A. Lasia, "Electrochemical Impedance Spectroscopy and its Applications", Springer, Heidelberg, Dordrecht, London (2014).
- 15) B. A. Boukamp, *J. Electrochem. Soc.*, **142**, 1885–1894 (1995).
- 16) M. Schönleber, D. Klotz and E. Ivers-Tiffée, *Electrochim. Acta*,

- 131, 20–27 (2014).
- 17) <http://www.iam.kit.edu/wet/english/Lin-KK.php> (2015).
- 18) E. R. v. Schweidler, *Ann. Phys.*, **329**, 711–770 (1907).
- 19) K. W. Wagner, *Ann. Phys.*, **345**, 817–855 (1913).
- 20) R. M. Fuoss and J. G. Kirkwood, *J. Am. Chem. Soc.*, **63**, 385–394 (1941).
- 21) D. L. Misell and R. J. Sheppard, *Journal of Physics D: Applied Physics*, **6**, 379–389 (1973).
- 22) K. Giese, *Advances in Molecular Relaxation Processes*, **5**, 363–373 (1973).
- 23) P. Colonomos and R. G. Gordon, *The Journal of Chemical Physics*, **71**, 1159–1166 (1979).
- 24) J. L. Salefran and Y. Dutuit, *The Journal of Chemical Physics*, **74**, 3056–3063 (1981).
- 25) A. D. Franklin and H. J. de Bruin, *Physica Status Solidi A*, **75**, 647–676 (1983).
- 26) F. D. Morgan and D. P. Lesmes, *The Journal of Chemical Physics*, **100**, 671–681 (1994).
- 27) K. S. Paulson, S. Jouravleva and C. N. McLeod, *IEEE transactions on biomedical engineering*, **47**, 1510–1517 (2000).
- 28) H. Schichlein, A. C. Müller, M. Voigts, A. Krügel and E. Ivers-Tiffée, *Journal of Applied Electrochemistry*, **32**, 875–882 (2002).
- 29) M. Schönleber and E. Ivers-Tiffée, *Electrochemistry Communications*, **58**, 15–19 (2015).
- 30) V. Sonn, A. Leonide and E. Ivers-Tiffée, *J. Electrochim. Soc.*, **155**, B675–B679 (2008).
- 31) C. W. Groetsch, “The Theory of Tikhonov Regularization for Fredholm Equations of the First Kind”, Pitman Publishing, Boston (1986).
- 32) A. N. Tikhonov, Goncharsky, Stepanov and Yagola, “Numerical Methods for the Solution of Ill-Posed Problems”, Kluwer Academic Publishers, Dordrecht, Boston, London (1990).
- 33) <http://cpc.cs.qub.ac.uk/summaries/ACGH.v1.0.html> (1992).
- 34) J. Weese, *Computer Physics Communications*, **69**, 99–111 (1992).
- 35) C. Graves, S. D. Ebbesen and M. Mogensen, *Solid State Ionics*, **192**, 398–403 (2011).
- 36) Z. Wuillemin, Y. Antonetti, C. Beetschen, O. Millioud, S. Ceschin, H. Madi and J. van Herle, *ECS Trans.*, **57**, 561–570 (2013).
- 37) H. Sumi, T. Yamaguchi, K. Hamamoto, T. Suzuki and Y. Fujishiro, *Solid State Ionics*, **262**, 407–410 (2014).
- 38) F. Ciucci and C. Chen, *Electrochim. Acta*, **167**, 439–454 (2015).
- 39) Y. Zhang, Y. Chen, M. Li, M. Yan, M. Ni and C. Xia, *J. Power Sources*, **308**, 1–6 (2016).
- 40) V. Subotic, C. Schluckner, J. Strasser, V. Lawlor, J. Mathe, J. Rechberger, H. Schroettner and C. Hochenauer, *Electrochim. Acta*, **207**, 224–236 (2016).
- 41) A. Nechache, A. Mansuy, M. Petitjean, J. Mougin, F. Mauvy, B. A. Boukamp, M. Cassir and A. Ringueude, *Electrochim. Acta*, **210**, 596–605 (2016).
- 42) K. Kobayashi, Y. Sakka and T. S. Suzuki, *J. Ceram. Soc. Japan*, **124**, 943–949 (2016).
- 43) S. Katayama, H. Nakai and A. Kita, *Meeting Abstracts, MA2016-02* (3), p. 324 (2016).
- 44) J. P. Schmidt, P. Berg, M. Schönleber, A. Weber and E. Ivers-Tiffée, *J. Power Sources*, **221**, 70–77 (2013).
- 45) M. Hanke and P. C. Hansen, *Surv. Math. Ind.*, **3**, 253–315 (1993).
- 46) A. Leonide, “SOFC Modelling and Parameter Identification by means of Impedance Spectroscopy”, KIT Scientific Publishing, Karlsruhe (2010).
- 47) C. Endler, A. Leonide, A. Weber, F. Tietz and E. Ivers-Tiffée, *J. Electrochim. Soc.*, **157**, B292–B298 (2010).
- 48) D. Klotz, J. P. Schmidt, A. Kromp, A. Weber and E. Ivers-Tiffée, *ECS Trans.*, **41**, 25–33 (2012).
- 49) A. Leonide, V. Sonn, A. Weber and E. Ivers-Tiffée, *J. Electrochim. Soc.*, **155**, B36–B41 (2008).
- 50) J. Hayd and E. Ivers-Tiffée, *J. Electrochim. Soc.*, **160**, F1197–F1206 (2013).
- 51) A. Leonide, S. Hansmann and E. Ivers-Tiffée, *ECS Trans.*, **28**, 341–346 (2010).
- 52) A. Leonide, S. Hansmann, A. Weber and E. Ivers-Tiffée, *J. Power Sources*, **196**, 7343–7346 (2011).
- 53) J. Illig, “Physically based Impedance Modelling of Lithium-Ion Cells”, KIT Scientific Publishing, Karlsruhe (2014).
- 54) A. Leonide, B. Rüger, A. Weber, W. A. Meulenberg and E. Ivers-Tiffée, *J. Electrochim. Soc.*, **157**, B234–B239 (2010).
- 55) P. Blennow, J. Hjelm, T. Klemensoe, S. Ramousse, A. Kromp, A. Leonide and A. Weber, *J. Power Sources*, **196**, 7117–7125 (2011).
- 56) Q. Ma, F. Tietz, A. Leonide and E. Ivers-Tiffée, *J. Power Sources*, **196**, 7308–7312 (2011).
- 57) F. Han, R. Mücke, T. van Gestel, A. Leonide, N. H. Menzler, H. P. Buchkremer and D. Stöver, *J. Power Sources*, **218**, 157–162 (2012).
- 58) A. Kromp, A. Leonide, A. Weber and E. Ivers-Tiffée, *J. Electrochim. Soc.*, **158**, B980–B986 (2011).
- 59) A. Kromp, S. Dierickx, A. Leonide, A. Weber and E. Ivers-Tiffée, *J. Electrochim. Soc.*, **159**, B597–B601 (2012).
- 60) S. Dierickx, A. Weber and E. Ivers-Tiffée, in 12th European SOFC & SOE Forum 2016, NN, Editor, NaN, p. B0502 (2016).
- 61) J. Joos, M. Ender, I. Rotscholl, N. Menzler, A. Weber and E. Ivers-Tiffée, *J. Power Sources*, **246**, 819–830 (2014).
- 62) A. Utz, H. Störmer, A. Leonide, A. Weber and E. Ivers-Tiffée, *J. Electrochim. Soc.*, **157**, B920–B930 (2010).
- 63) V. Sonn and E. Ivers-Tiffée, in Proceedings of the 8th European Solid Oxide Fuel Cell Forum, R. Steinberger-Wilckens and U. Bossel, Editors, p. B1005 (2008).
- 64) B. Butz, A. Lefarth, H. Störmer, A. Utz, E. Ivers-Tiffée and D. Gerthsen, *Solid State Ionics*, **214**, 37–44 (2012).
- 65) J. P. Schmidt, T. Chrobak, M. Ender, J. Illig, D. Klotz and E. Ivers-Tiffée, *J. Power Sources*, **196**, 5342–5348 (2011).
- 66) J. Illig, M. Ender, T. Chrobak, J. P. Schmidt, D. Klotz and E. Ivers-Tiffée, *J. Electrochim. Soc.*, **159**, A952–A960 (2012).
- 67) J. Illig, J. P. Schmidt, M. Weiss, A. Weber and E. Ivers-Tiffée, *J. Power Sources*, **239**, 670–679 (2013).
- 68) J. Illig, T. Chrobak, M. Ender, J. P. Schmidt, D. Klotz and E. Ivers-Tiffée, *ECS Trans.*, **28**, 3–17 (2010).
- 69) M. D. Levi and D. Aurbach, *Journal of Physical Chemistry B*, **101**, 4630–4640 (1997).
- 70) D. Klotz, M. Schönleber, J. P. Schmidt and E. Ivers-Tiffée, *Electrochim. Acta*, **56**, 8763–8769 (2011).
- 71) J. Illig, M. Ender, A. Weber and E. Ivers-Tiffée, *J. Power Sources*, **282**, 335–347 (2015).
- 72) M. Ender, A. Weber and E. Ivers-Tiffée, *Electrochemistry Communications*, **34**, 130–133 (2013).
- 73) M. Ender, J. Joos, A. Weber and E. Ivers-Tiffée, *J. Power Sources*, **269**, 912–919 (2014).
- 74) C. Endler-Schuck, J. Joos, C. Niedrig, A. Weber and E. Ivers-Tiffée, *Solid State Ionics*, **269**, 67–79 (2015).
- 75) M. Kornely, N. H. Menzler, A. Weber and E. Ivers-Tiffée, *Fuel Cells*, **13**, 506–510 (2013).
- 76) M. Kornely, A. Neumann, N. Menzler, A. Leonide, A. Weber and E. Ivers-Tiffée, *J. Power Sources*, **196**, 7203–7208 (2011).
- 77) A. Weber, S. Dierickx, A. Kromp and E. Ivers-Tiffée, *Fuel Cells*, **13**, 487–493 (2013).
- 78) Q. MA, F. Tietz, A. Leonide and E. Ivers-Tiffée, *ECS Trans.*, **35**, 1421–1433 (2011).
- 79) A. Leonide, A. Weber and E. Ivers-Tiffée, *ECS Trans.*, **35**, 2961–2968 (2011).
- 80) Q. Fang, L. Blum and N. H. Menzler, *J. Electrochim. Soc.*, **162**, F907–F912 (2015).